Spring 2022

Proline to Serine Mutation in the Active Site Loop of Malate Dehydrogenase Alters Substrate Specificity

Olivia J. Schmitt
Providence College

Proline to serine mutation in the active site loop of malate dehydrogenase alters substrate specificity

Submitted May 17, 2021

Olivia J. Schmitt, Tyler Stack, and Kathleen Cornely

From the Department of Chemistry and Biochemistry, Providence College, Providence, RI 02918

Cancer cells preferentially undergo glycolysis in aerobic environments, a phenomenon termed the Warburg effect. Malate dehydrogenase (MDH) catalyzes the reversible interconversion of malate and oxaloacetate. Human cytosolic malate dehydrogenase (hMDH1) isoform 3 is involved in the malate-aspartate shuttle (MAS), which oxidizes cytosolic NADH. hMDH1 is implicated in high aerobic glycolysis in cancer cells because NAD is a necessary cofactor for glycolysis. Thus, hMDH1 is a promising molecular target for cancer treatment. A single proline residue at position 110 in the mobile active site loop of hMDH1 was mutated to a serine with the intention of altering the enzyme's substrate specificity. Steady-state kinetics analysis showed that mutant activity with the native substrate, oxaloacetate, exceeded that of the wildtype (WT) enzyme (k_{cat} of 320 ± 10 s^{-1} and 780 ± 30 s^{-1} for the WT and mutant, respectively). Catalytic activity of both enzymes decreased significantly with the alternative substrate, α-ketoglutarate (k_{cat} of 3 ± {6} s^{-1} and 0.19 ± 0.01 s^{-1} for the WT and mutant, respectively). The specificity constant ($k_{sp} = k_{cat}/K_M$) signifies the efficiency of an enzyme for competing substrates. The k_{sp} values for the WT and mutant with OAA were 1.7 ± 0.2 × 10^7 $M^{-1}s^{-1}$ and 8.21 ± 0.46 × 10^6 $M^{-1}s^{-1}$, respectively. These k_{sp} values were substantially higher than those for both enzymes with α-ketoglutarate. We can conclude that the WT and mutant hMDH1 enzymes function optimally with oxaloacetate. Also, Pro110Ser hMDH1 has altered substrate specificity, with α-ketoglutarate functioning as an alternative substrate.

Warburg metabolism is a hallmark of cancer cells (1). Even in the presence of sufficient oxygen, cancer cells use glycolysis for energy synthesis. In a process known as the Crabtree effect, the glycolytic pathway is detached from the citric acid (TCA) cycle (2). During glycolysis, a single glucose molecule is converted to two pyruvates. In healthy cells and under aerobic conditions, pyruvate is oxidized to acetyl-coenzyme A (acetyl-CoA), which may enter the TCA cycle in the mitochondrial matrix. However, cancer cells upregulate the enzyme lactate dehydrogenase (LDH) [EC 1.1.1.27], which produces lactate from pyruvate and regenerates NAD for glycolysis (3). LDH alone is insufficient to produce adequate amounts of the cofactor NAD (3). The activity of cytosolic malate dehydrogenase (MDH1) [EC 1.1.1.37] is also necessary for NAD production (4). Cancer cells overexpress both LDH and MDH1 to meet the NAD demands for sustained glycolysis.

Upregulation of glycolysis in cancer cells is further evidenced by the overexpression of key glycolytic proteins, including phosphofructokinase-1 (PFK1), glucose transporters (GLUT), hexokinase II (HKII), pyruvate dehydrogenase kinase (PDK), and pyruvate kinase M2 (PKM2) (5). Activation of these enzymes increases glucose migration into the cell and enhances the glycolytic pathway, ultimately contributing to tumorigenesis. Although the evolutionary advantages of aerobic glycolysis remain uncertain, it is probable that the glycolytic pathway provides intermediates for other metabolic pathways, including fatty acid synthesis and the pentose phosphate pathway (PPP), serving to increase the biomass of cancer cells (5). For instance, glucose-6-phosphate (G6P), an intermediate molecule in the glycolytic pathway, can be oxidized to 6-phosphoglucono-lactone, which can then enter other metabolic pathways,

including the PPP. Growing evidence also suggests that increased glycolysis correspondingly increases the rate of ATP synthesis, which is advantageous for cancer cell proliferation (5).

While the role of LDH in NAD production is well established, that of hMDH1 is more ambiguous. Distinct isoforms of MDH differ in their subcellular localizations. hMDH1 is implicated in the malate-aspartate shuttle (MAS), which carries electrons from the cytosol into the mitochondrial matrix through malate (4). Thus, MAS transports equivalents from cytosolic NADH into the mitochondria (6). This shuttle system ultimately regenerates NAD in the cytosol, which is again necessary for continued glycolysis. Reducing or manipulating hMDH1 activity may serve as a potential treatment for cancer.

Here we report the results of the production, purification, and characterization of a novel mutant hMDH1 protein. Kinetics analysis suggests that the mutant enzyme is more active than the WT with the endogenous oxaloacetate (OAA) substrate, as it has a higher turnover number (k_{cat}). The WT enzyme has greater proficiency with OAA than does the mutant, suggested by the higher specificity constant (k_{sp}) of the WT. Both the WT and the mutant are significantly less active with the alternative substrate, α-ketoglutarate (AKG), a key molecule in the Krebs cycle. However, the mutant enzyme is likely more active and proficient with AKG, relative to the WT. Together, this information suggests that residue Pro-110 within the active site loop of hMDH1 is a potential candidate for altered catalytic activity and substrate specificity of this enzyme.

Results

Mutation selection within the active site loop

Since there is no solved structure of the human cytosolic malate dehydrogenase 1 (hMDH1) enzyme [P40925-3], a model structure based on the porcine MDH enzyme [PDB: 5MDH] was analyzed. PyMOL Molecular Graphics Service System (7) was used to visualize the mobile loop that bends into the active site of the enzyme (Fig. 1). Catalytic residues within this loop drive the reversible interconversion of malate and oxaloacetate (OAA). Once the substrate binds, the loop closes, and catalysis begins. Evaluation of the loop revealed a rigid proline amino acid residue at position 110 (Fig. 2*A*). Mutation numbering is based on the protein produced by the plasmid. In order to enhance the flexibility of the loop, a serine residue was introduced at position 110 (Fig. 2*B*). The mutagenesis tool in PyMOL was used for this purpose.

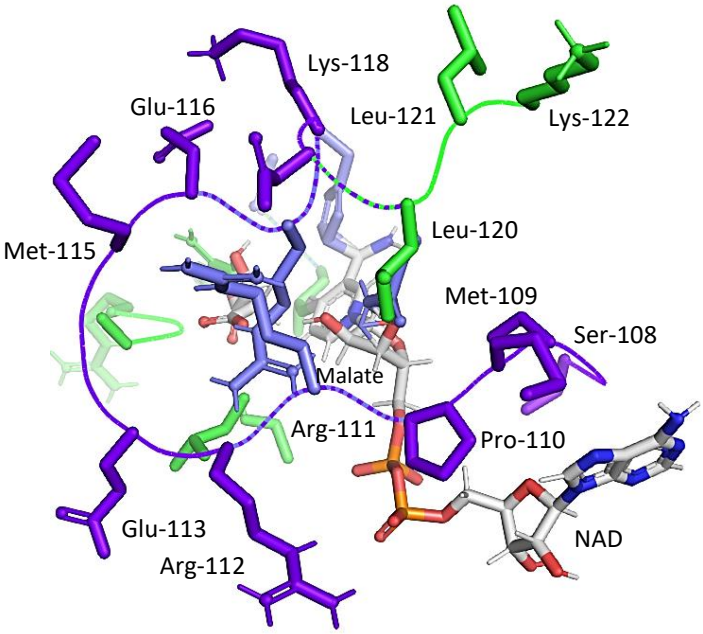

Figure 1. PyMOL generated visual of MDH1 loop. This image displays the residues situated in the mobile active site loop of MDH1 [PDB: 5MDH]. Porcine MDH was used as a model for the human enzyme. The loop closes around its substrate and orients it in the correct position for productive catalysis. Loop residues are shown in purple. Malate is featured in the back of the image. The oxidized cofactor, NAD, is shown as well.

WT plasmid DNA purification

hMDH1 isoform 3 pET28a plasmid DNA was extracted from *Escherichia coli* (*E. coli*) BL21(DE3) cells and analyzed using a microvolume spectrophotometer. The 260/280 and 260/230 ratios indicate nucleic acid purity. The A_{260}/A_{280} ratio was 1.90, which falls within the 1.8-2.0 range that is generally accepted as "pure" for DNA (Fig. 3). This suggests the absence of protein in the DNA sample and that it is pure. Expected

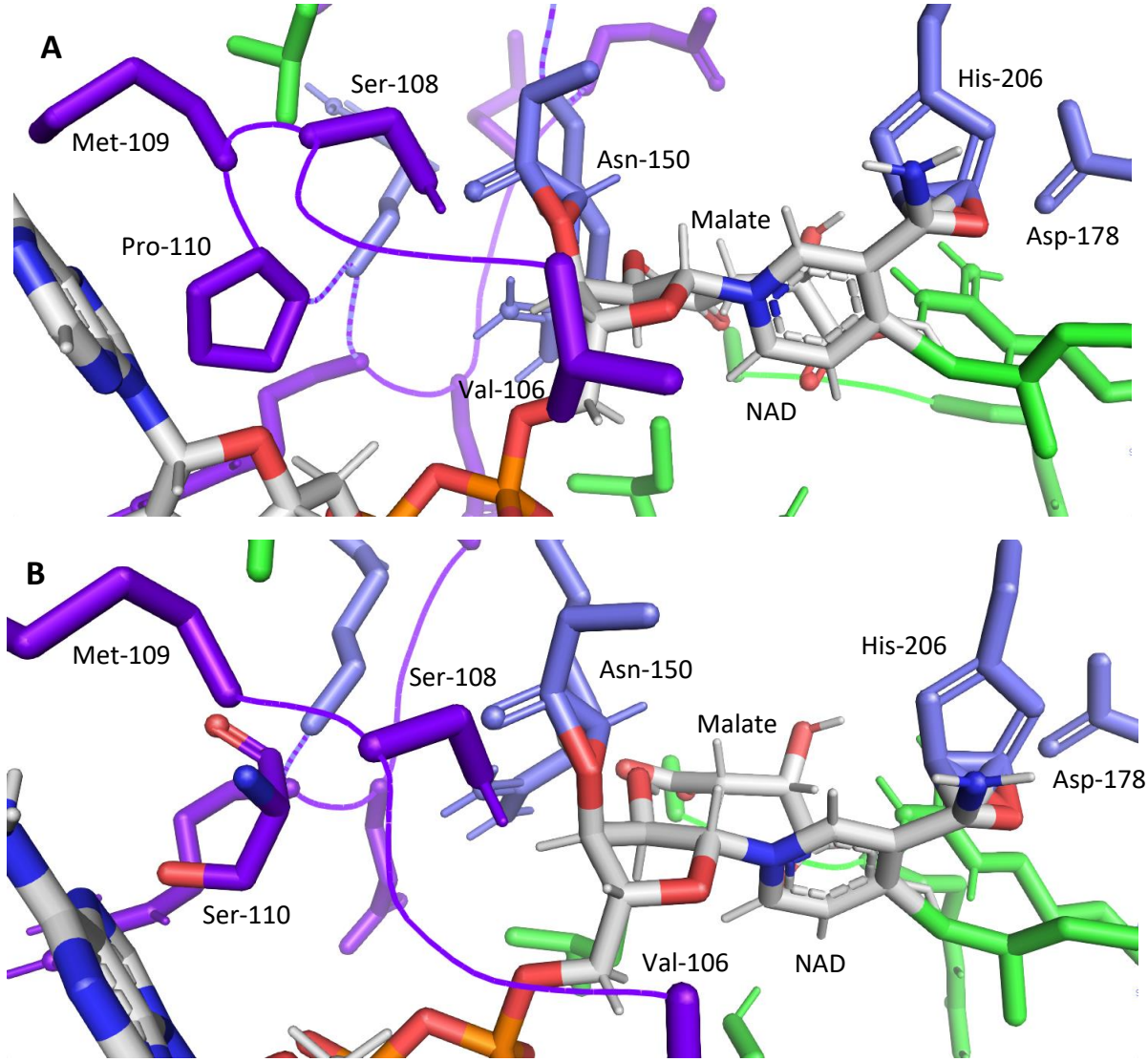

Figure 2. PyMOL generated image of proline to serine mutation. *(A)* The proline residue at position 110 in the mobile active site loop of hMDH1 was replaced with a serine. Proximity of Pro-110 with the substrate, malate, and cofactor, NAD, is featured here. *(B)* The smaller serine amino acid residue was introduced to confer flexibility to the loop.

260/230 values for nucleic acids are commonly in the range of 2.0-2.2. The 260/230 ratio was 1.93, which is only moderately lower than the accepted value for pure DNA. The low ratio is reflected in the high troughs on the graph plotting absorbance versus wavelength in nm. Finally, the DNA concentration was relatively high at 157.6 ng/µL.

Restriction enzymes

A double restriction analysis (Fig. 4) was performed to verify the existence of the WT pET28a plasmid. The restriction enzymes XhoI and ClaI digested the plasmid DNA for about 30 minutes. The digest was expected to produce two distinct DNA fragments at 4.9 kb and 1.4 kb, respectively. These were the expected fragment sizes based on bioinformatics work in Benchling. Gel electrophoresis analysis revealed a single, bright band and a faint band of cut DNA (Fig. 4, *lane 2*).

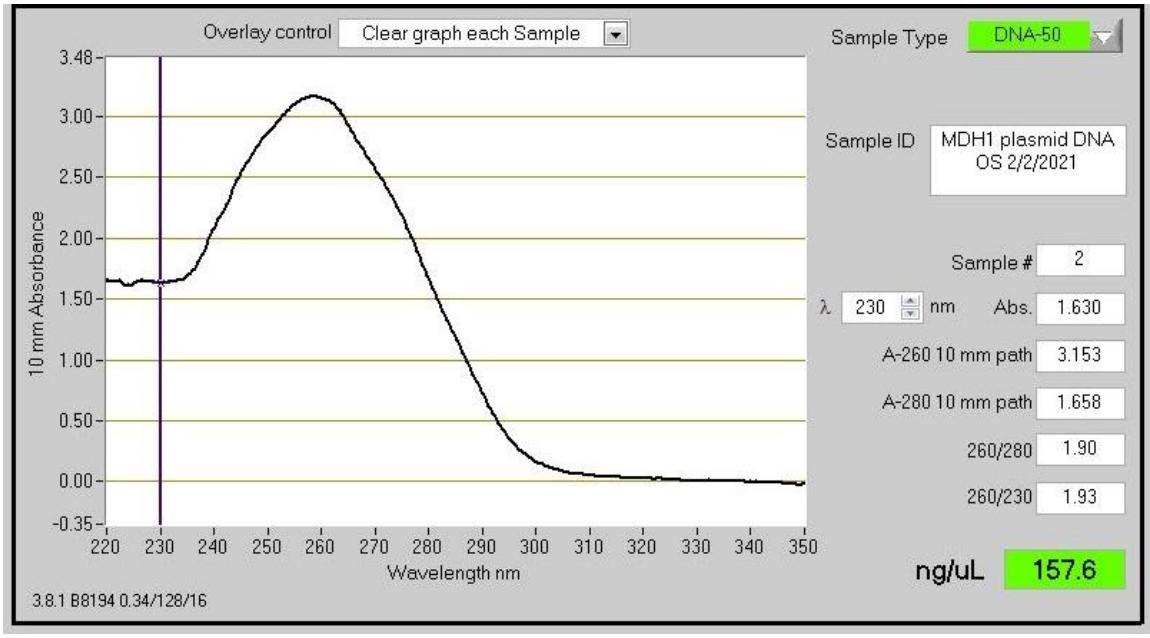

Figure 3. WT hMDH1 plasmid DNA data. Once the WT hMDH1 isoform 3 pET28 plasmid DNA was extracted from *E. coli* BL21(DE3) cells, the concentration was determined using a microvolume spectrophotometer. The DNA concentration was 157.6 ng/µL.

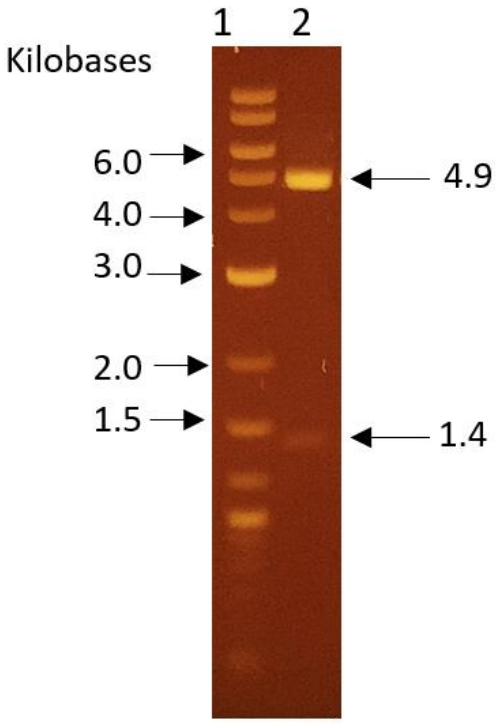

Figure 4. Restriction enzyme analysis. A double restriction digest was performed on the WT hMDH1 isoform 3 pET28a plasmid DNA with the restriction enzymes XhoI and ClaI. Lane 1 depicts the ladder and lane 2 features the cut WT plasmid DNA. Two distinct bands are shown in lane 2.

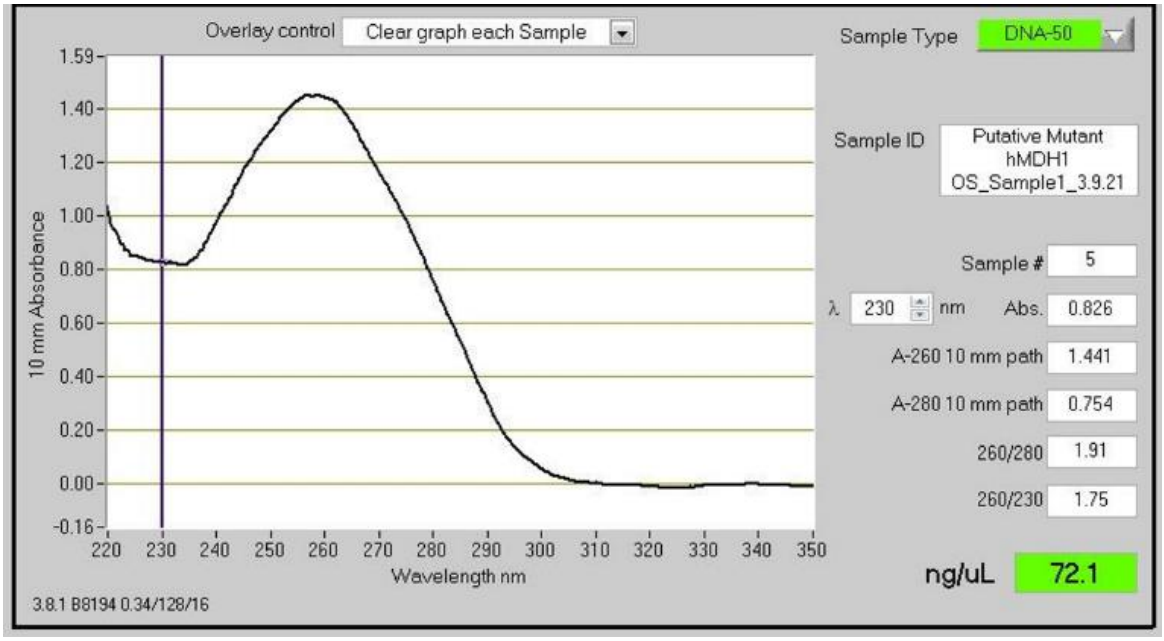

Figure 5. Putative hMDH1 mutant plasmid DNA data. Once the potential mutant hMDH1 isoform 3 pET28 plasmid DNA was extracted, the concentration was determined with a microvolume spectrophotometer. The DNA concentration was 72.1 ng/µL.

Site-directed mutagenesis and transformation of competent E. coli cells

After the presence of the WT pET28a plasmid was verified via restriction analysis, site-directed mutagenesis was employed to produce the Pro110Ser mutation. Polymerase Chain Reaction (PCR) was performed on the WT plasmid to introduce three new nucleotides at position 110 in the gene encoding hMDH1. The correct size of the fragment (6.292 kilobases) was confirmed with gel electrophoresis. A kinase, ligase, and DpnI (KLD) treatment was used to recircularize the plasmid. Competent NEB 5a *E. coli* cells were next transformed with the putative mutant plasmid. The transformants are potential bacterial colonies that took up the putative mutant hMDH1 plasmid (Fig. 6).

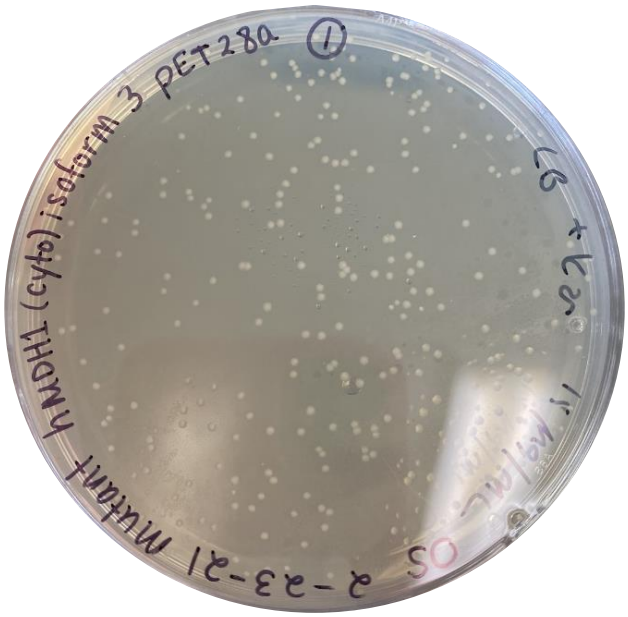

Figure 6. Transformation of 5α *E. coli* cells. Following PCR to introduce a substitution mutation (Pro110Ser) into the WT hMDH1 plasmid, a kinase, ligase, and DpnI (KLD) treatment was performed to recircularize the putative mutant hMDH1 isoform 3 pET28a plasmid. A transformation was completed to introduce the putative mutant hMDH1 plasmid into competent NEB 5α *E. coli* cells.

Mutant plasmid DNA purification

The putative mutant plasmid DNA extracted from BL21(DE3) cells was pure. The DNA concentration was relatively high at 72.1 ng/µL. The 260/280 and 260/230 ratios (Fig. 5) indicate nucleic acid purity. The A_{260}/A_{280} ratio was

1.91, which falls within the recommended 1.8-2.0 range for "pure" DNA. Expected 260/230 values for nucleic acids are commonly in the range of 2.0-2.2. The 260/230 ratio was 1.75, which was lower than that accepted for pure DNA. The low ratio is reflected in the high troughs on the graph plotting absorbance versus wavelength in nm. The putative mutant plasmid DNA may contain some contaminants.

Mutant plasmid confirmation

The putative mutant plasmid DNA extracted from BL21(DE3) cells was sent to GeneWiz for sequencing. The sequencing results revealed the correct substitution of three nucleotides (CCA), which encode proline, with three different nucleotides (AGC), which encode serine at position 110 in the hMDH1 isoform 3 gene.

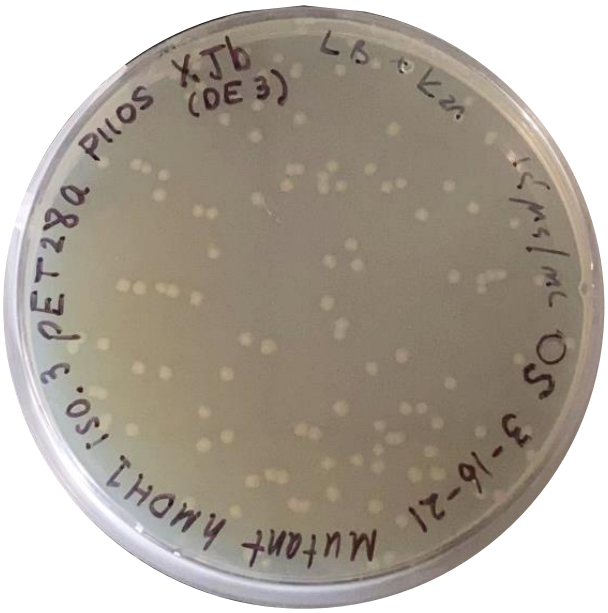

Figure 7. Bacterial transformation of XJb (DE3) cells. The plasmid encoding the gene for the genetically modified hMDH1 isoform 3 was introduced into XJb (DE3) bacterial cells.

Transformation of competent E. coli *cells*

The plasmid encoding the gene for the genetically modified hMDH1 mutant plasmid DNA was introduced into Xjb (DE3) Autolysis cells. Transformants on the plate are potential colonies that took up the mutant hMDH1 plasmid (Fig. 7). The transformation efficiency, defined as the number of transformants per unit mass of DNA on the plate, was 1.7×10^3 transformants/µg.

Protein overexpression, cell lysis, and purification

Transformation of Xjb (DE3) cells was followed by overexpression, in which the plasmid gene was used by the host bacterium to transcribe mRNA, followed by translation into protein. Both the WT plasmid and the plasmid encoding the gene for the genetically modified hMDH1 mutant plasmid DNA were overexpressed. Cells overexpressing the WT hMDH1 isoform 3 protein and the mutant protein were lysed to obtain a lysate that could be used to purify the protein by nickel affinity (Ni-NTA) chromatography. Both the WT and the mutant proteins eluted at an imidazole concentration of 250 mM in the chromatography experiment.

BCA assay on WT and mutant hMDH1

A bicinchoninic (BCA) assay was performed to determine the concentration of the WT and the mutant hMDH1 enzymes. The BCA standard solutions were used to construct a standard curve (Fig. 8). The concentrations of the WT and mutant proteins were determined from the standard curve (0.334 mg/mL and 0.44 ± 0.02 mg/mL, respectively).

SDS-PAGE analysis of WT and mutant hMDH1 proteins

SDS-PAGE was used to determine the molecular weights of the WT and mutant hMDH1 proteins. The molecular weights of the protein bands were determined by constructing a standard curve of the square root of the molecular weight of the ladder proteins versus the log of the distance each ladder protein band travelled from the top of the gel (Fig. 10). Distances were measured in centimeters. The resulting linear regression equation was used to determine the molecular weights of the proteins in the gel bands. Two

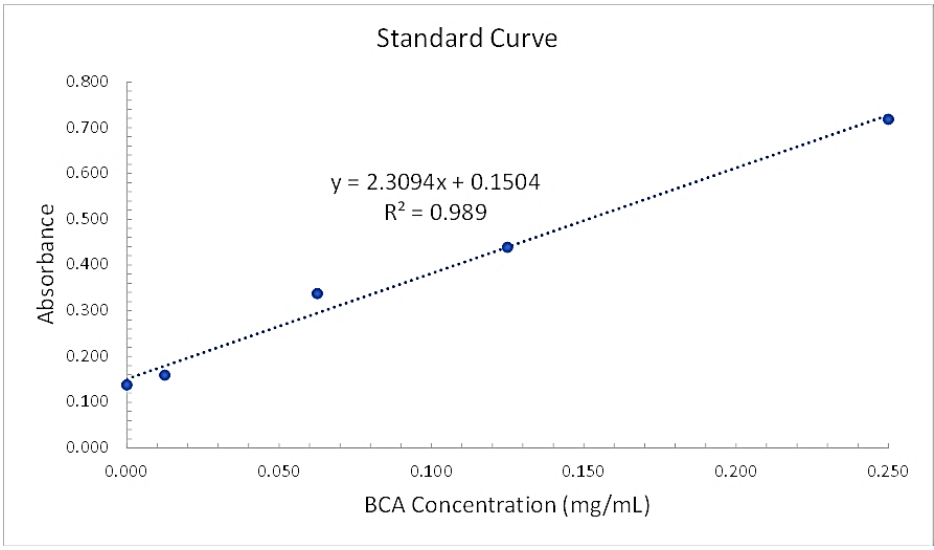

Figure 8. BCA assay for determining wildtype and mutant protein concentration. The absorbance measurements of a series of standard solutions of BCA were plotted against concentration to yield a linear standard curve. The concentration of the WT hMDH1 protein was determined to be 0.334 mg/mL, while that of the mutant was determined to be 0.44 ± 0.02 mg/mL.

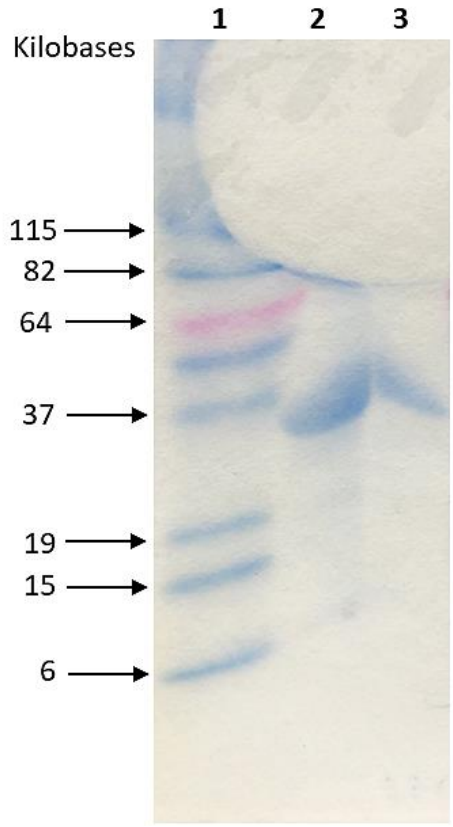

Figure 9. Protein analysis by SDS-PAGE. SDS-PAGE was used to determine the molecular weights of the WT and mutant hMDH1 proteins. SDS-PAGE also verified the success of the purification procedure. A sharp band occured at approximately 37 kDa for both the mutant (lane 2) and the WT (lane 3) samples.

prominent dark blue bands appeared on the gel, one for the mutant enzyme (Fig. 9, *lane 2*) and one for the WT enzyme (Fig 9, *lane 3*). The calculated molecular weight of the mutant protein was 34.8 kDa, whereas that of the WT protein was 39.4 kDa. These values match well with the expected molecular weights, confirming the presence of the purified proteins.

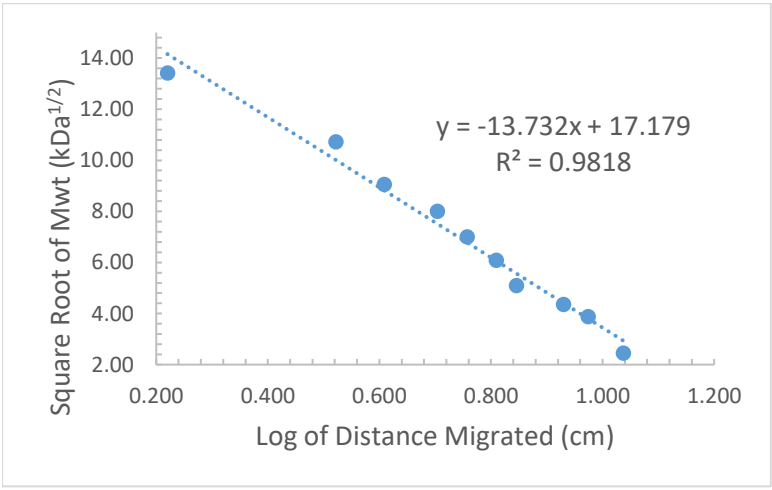

Figure 10. SDS-PAGE standard curve. A standard curve plotting square root of molecule weight of the ladder proteins as a function of the logarithm of the distance migrated by the ladder proteins was created. The molecular weights of the WT and mutant hMDH1 proteins were determined from the best-fit equation for the data.

Table 1
Steady-state kinetic parameters for WT hMDH1 with different substrates

Substrate	K_{cat} (s^{-1})	K_{sp} ($M^{-1}s^{-1}$)	K_M (µM)	t-Statistic (K_{cat})	t-Statistic (K_{sp})	P-Value (K_{cat})	P-Value (K_{sp})
OAA	320 ± 10	17 ± 2	18.4 ± 0.1	25.8799	8.51959	5.33277×10^{-9}	2.76856×10^{-5}
AKG	3 ± {6}	0.003 ± {0.008}	{1,098} ± 3	0.556613	0.360203	0.607462	0.736909

Table 2
Steady-state kinetic parameters for mutant hMDH1 with different substrates

Substrate	K_{cat} (s^{-1})	K_{sp} ($M^{-1}s^{-1}$)	K_M (µM)	t-Statistic (K_{cat})	t-Statistic (K_{sp})	P-Value (K_{cat})	P-Value (K_{sp})
OAA	780 ± 30	8.21 ± 0.46	95.33 ± 0.07	25.5726	17.8344	5.86153×10^{-9}	1.0007×10^{-7}
AKG	0.19 ± 0.01	0.00029 ± 0.00003	{666.2} ± 0.1	19.1259	9.21413	3.12139×10^{-4}	0.00270391

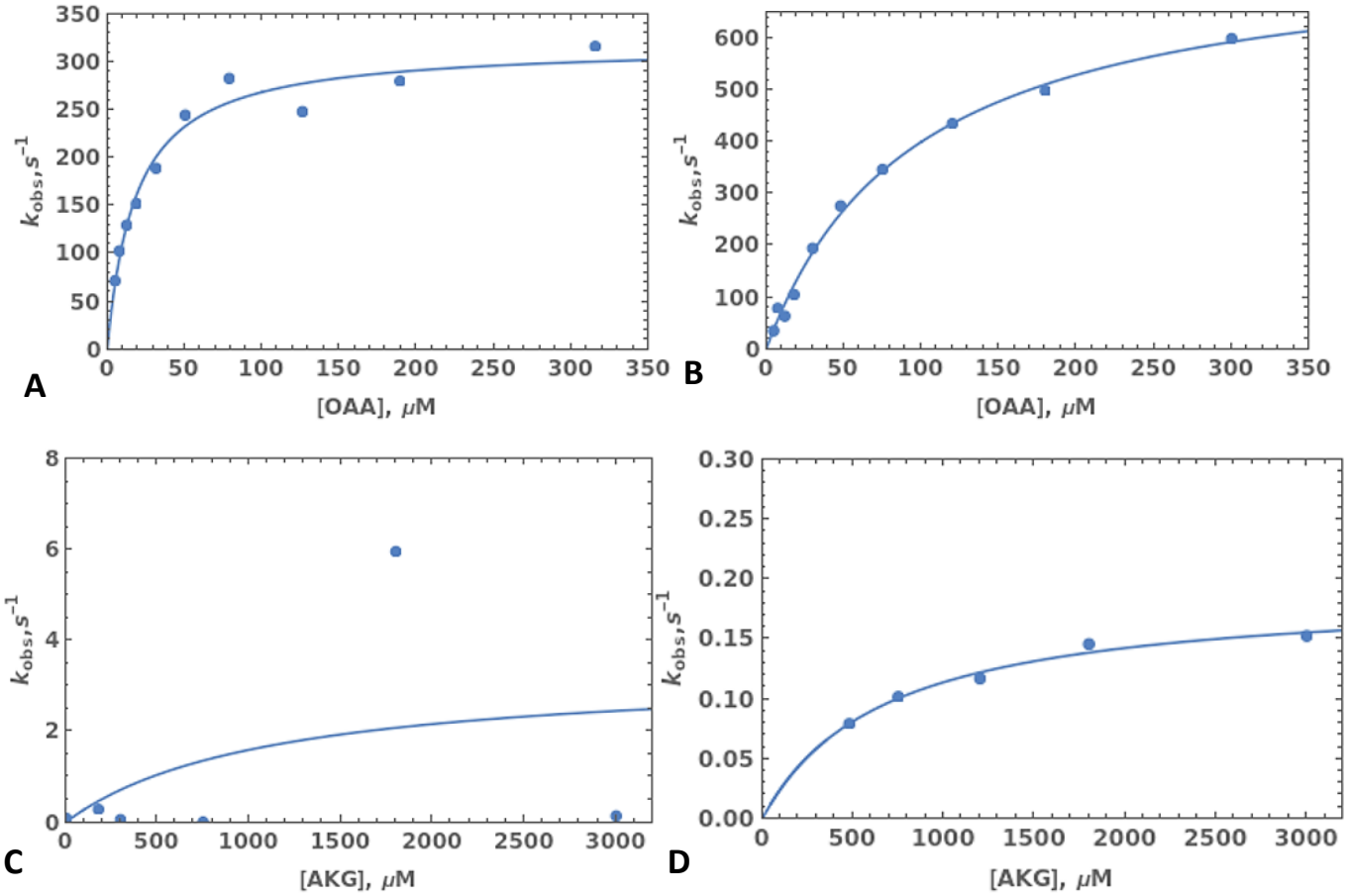

Figure 11. Mathematica plots for WT and mutant with OAA and AKG. Kinetics parameters were evaluated for the WT and the mutant enzyme in the presence of the native substrate, oxaloacetate (OAA), and an alternative substrate, α-ketoglutarate (AKG). *(A)* WT enzyme activity was evaluated with OAA. The data was fitted to a non-linear model. *(B)* Mutant hMDH1 enzyme activity was monitored with OAA. *(C)* The WT enzyme was treated with AKG, but the data was difficult to fit to a curve. *(D)* The mutant enzyme was treated with AKG.

Steady-state kinetics

The activities of both the WT and mutant hMDH1 were evaluated under steady-state conditions. The results show a k_{cat} of 320 ± 10 s^{-1} for the WT enzyme with the native substrate, OAA (Table 1). k_{cat} for the mutant enzyme with OAA (780 ± 30 s^{-1}) was roughly double that for the WT (Table 2). The K_M for the WT enzyme with OAA was 18.4 ± 0.1 µM, and the k_{sp} was 1.7 ± 2 × 10^7 $M^{-1}s^{-1}$ (Table 1). The K_M for the mutant enzyme with OAA was much higher at 95.33 ± 0.07 µM, and the k_{sp} was roughly half that of the WT, at 8.21 ± 0.46 ×10^6 $M^{-1}s^{-1}$ (Table 2). Enzyme activity and proficiency were studied with an alternative substrate, AKG. The k_{cat} of the WT enzyme with AKG was 3 ± {6} s^{-1} (Table 1). The K_M for the WT enzyme with AKG was {1,098} ± 3 µM, and the k_{sp} is 0.003 ± {0.008} × 10^6 $M^{-1}s^{-1}$ (Table 1). By contrast, the k_{cat} of the mutant enzyme with AKG was 0.19 ± 0.01 s^{-1} (Table 2). The K_M for the mutant enzyme with AKG was {666.2} ± 0.1 µM, and the k_{sp} was 0.00028 ± 0.00003 × 10^6 $M^{-1}s^{-1}$ (Table 2). The kinetic data were fitted using the online version of Wolfram Mathematica (8) to obtain the kinetic parameters (Fig. 11*A*, *B*, *C*, *D*).

Discussion

Site-directed mutagenesis was employed to construct a plasmid containing a mutant hMDH1 gene and to evaluate the role of conformational flexibility of the active site loop. Enhanced mobility of the loop was predicted to permit larger substrates, like α-ketoglutarate (AKG), to fit into the binding pocket. The PyMOL images of the mobile active site loop of hMDH1 display a diverse range of residues, which likely influence the flexibility of the loop and its catalytic properties (Fig. 1). Residues in the loop region are conserved across taxa, but not all residues are essential for catalysis (9). Residues, like active site arginines, that are critical for substrate orientation and enzyme reactivity were likely poor candidates for mutagenesis. With the intention of altering substrate recognition, the proline amino acid residue located at position 110 of the hMDH1 gene was replaced with a serine. Note that the mutation numbering is based on the protein produced by the plasmid, which contains an N-terminal glycine. Proline is arguably the most rigid amino acid residue, since its side chain is connected to the protein backbone twice. Serine, on the other hand, is more flexible because it lacks a ring, and its side chain is relatively small. Replacing a rigid, moderately bulky side chain with a smaller side chain was hypothesized to increase the flexibility of the loop, allowing it to accommodate longer substrates like AKG. Serine was chosen with the intention of introducing hydrogen bonding contacts in the active site, which might contribute to transition state stabilization in the conversion from substrate to product. However, no polar contacts were formed, likely because serine was situated too far from other residues in the loop (Fig. 2*B*).

WT hMDH1 isoform 3 pET28a plasmid DNA was extracted from *E. coli* BL21(DE3) cells. The WT plasmid was purified and analyzed using a microvolume spectrophotometer (Fig. 3). The 260/280 and 260/230 ratios were assessed to determine nucleic acid purity. The 260/280 ratio was 1.90, which falls within the expected range for "pure" DNA (1.8-2.0). The proper ratio suggests the absence of protein in the DNA sample and that it is pure. A 260/280 ratio of about 2.0 is generally accepted as "pure" for RNA. Since the ratio is slightly higher than 1.8, the DNA might contain a small amount of RNA. Expected 260/230 values for nucleic acids are commonly in the range of 2.0-2.2. The 260/230 ratio was 1.93, which is slightly lower than the accepted value for pure DNA. The high troughs on the graph plotting absorbance versus wavelength in nm reflect this low ratio. The WT plasmid DNA may contain some contaminants, such as genomic DNA. Perhaps the cells were subjected to mechanical stress during the extraction experiment. Finally, the DNA yield was relatively high at 157.6 ng/µL.

The double restriction digest results verify the presence of the WT pET28a plasmid DNA and suggest that it is of high quality and concentration. The restriction enzymes XhoI and ClaI were used to fragment the plasmid DNA. XhoI recognizes the DNA sequence C/TCGAG. The DNA recognition sequence for ClaI is AT/CGAT. The first band of

cut DNA (Fig. 4, *lane 2*) is sharp and bright, whereas the second band of cut DNA (Fig. 4, *lane 2*) is slightly fainter. The faint DNA band is likely a consequence of the difficulty of visualizing smaller fragments on a gel. The bands appear at the expected fragment sizes of 4.9 kb and 1.4 kb, determined from the bioinformatics platform, Benchling (10). These results suggest that the WT hMDH1 plasmid was successfully amplified.

Site-directed mutagenesis of the WT pET28a plasmid was next performed. PCR was used to amplify the plasmid DNA and introduce the Pro110Ser mutation. The PCR results suggest that mutagenesis was successful, as a band appeared at the correct fragment size of 6.292 kilobases. The putative mutant hMDH1 isoform 3 pET28a plasmid was recircularized with a KLD treatment. Finally, competent NEB 5α *E. coli* cells were transformed with the putative mutant hMDH1 plasmid (Fig. 6). Many small colonies appear on the plate, suggesting that the transformation was successful.

To eventually verify the presence of the desired mutation, the putative mutant plasmid DNA was extracted and purified from BL21(DE3) cells. The DNA concentration was relatively high at 72.1 ng/μL (Fig. 5). The 260/280 and 260/230 ratios indicate plasmid purity. The A_{260}/ A_{280} ratio falls within the recommended range (1.8-2.0) for "pure" DNA, at 1.91. This indicates the absence of protein in the DNA sample and that it is pure. However, because the ratio is slightly higher than 1.8, the DNA might have a small amount of RNA in it. A high 260/280 ratio is not usually indicative of a problem, however. Expected 260/230 values for nucleic acids are commonly in the range of 2.0-2.2. The 260/230 ratio was 1.75, which is lower than that accepted for pure DNA. The low ratio is reflected in the high troughs on the graph plotting absorbance versus wavelength in nm. The putative mutant plasmid DNA may contain some contaminants including genomic DNA.

The putative mutant plasmid DNA extracted from BL21(DE3) cells was sent to GeneWiz for sequencing. The sequencing results indicate the correct substitution of three nucleotides (CCA), which encode proline, with three alternative nucleotides (AGC), which encode serine, at position 110 in the hMDH1 isoform 3 gene. The plasmid encoding the gene for the genetically modified hMDH1 isoform 3 was next introduced into XJb (DE3) bacterial cells. These cells are designed to take up protein efficiently. Small colonies on the plate suggest that the bacteria successfully took up the mutant plasmid (Fig. 7). However, small "satellite" colonies that grew where kanamycin had been broken down by the larger antibiotic-resistant transformed colonies appeared on the plate. The satellite colonies were non-transformed cells that surrounded larger transformed colonies. These satellite colonies were not included in the determination of transformation efficiency, nor were they used in future culture inoculation. The transformation efficiency was 1.7×10^3 transformants/μg, which lies just outside of the expected range of 10^4-10^7 transformants/μg.

Transformation of XJb (DE3) autolysis cells was followed by overexpression of the mutant hMDH1 isoform 3 protein. Cells overexpressing the mutant protein were isolated as a cell lysate. The lysate was purified by Ni-NTA chromatography. The same overexpression, lysis, and purification sequence was performed for the WT hMDH1 enzyme. Protein concentrations were determined by the Bicinchoninic (BCA) assay, which uses a standard curve of BCA standard solutions (Fig. 8). The correlation coefficient of the standard curve was high at 0.989, indicating that a linear fit was appropriate for the data. The mutant protein concentration was 0.44 ± 0.02 mg/mL. The WT protein concentration was lower at 0.334 mg/mL. The standard deviation for the mutant hMDH1 concentration was low at 0.02 mg/mL, suggesting that the concentration was determined precisely from the BCA standard curve.

The SDS-PAGE results suggest that the WT and the mutant hMDH1 proteins were successfully purified. A single, dark band exists for both enzymes at approximately 37 kDa (Fig. 9). Upward curving of the protein bands on both sides of the gel was likely caused by uneven temperature over the whole gel. The calculated molecular weight for the WT protein was 39.4 kDa, whereas that for the mutant was 34.8 kDa. The exact molecular weights of the WT and

mutant hMDH1 enzymes are 39.749 kDa and 39.739 kDa, respectively. The molecular weights determined via standard curve analysis (Fig. 10) were lower than the expected values. Increased interactions between the respective protein and sodium dodecyl sulfate (SDS) may have increased the surrounding negative charge on the protein, causing it to travel further down the gel (11). This would explain the slightly lowered molecular masses of the two enzymes.

The kinetics parameters of the WT and the purified recombinant hMDH1 protein were determined spectrophotometrically. Enzyme activity, specificity, and proficiency were evaluated. Values for k_{cat} and k_{cat}/K_M (k_{sp}) were deemed the most useful parameters for quantitative analysis of both enzymes (13). The k_{cat} of the WT enzyme with the endogenous substrate (OAA) was 320 ± 10 s^{-1} (Table 1). This number reflects values reported in the literature (11, 12). The K_M for the WT enzyme with OAA was 18.4 ± 0.1 µM, and the k_{sp} was $1.7 \pm 2 \times 10^7$ $M^{-1}s^{-1}$. By contrast, the k_{cat} of the mutant enzyme with OAA was 780 ± 30 s^{-1} (Table 2). The K_M for the mutant enzyme with OAA was 95.33 ± 0.07 µM, and the k_{sp} was $8.21 \pm 0.46 \times 10^6$ $M^{-1}s^{-1}$. The higher k_{cat} of the mutant with OAA indicates that more substrate molecules were transformed into product per unit time by a single mutant enzyme compared to the wildtype. The higher k_{sp} for the WT suggests that this enzyme is more effective on OAA than is the mutant. Loss of specificity for the native substrate was expected for the mutant enzyme, as it was hypothesized that Pro-110 is involved in substrate recognition in the mobile active site loop. While OAA binds more easily to the WT enzyme, it is converted to malate at a slower rate. The higher K_M for the mutant enzyme suggests that the nature of the enzyme-substrate complex (ES) was altered. There was likely a higher activation energy barrier for formation of the ES in the reaction scheme for the mutant enzyme with OAA. Decreasing the stability of the ES likely allowed for the malate product to be released from the enzyme's active site sooner.

The activities of the WT and mutant enzymes were assayed in the presence of the alternative substrate, α-ketoglutarate (AKG). The k_{cat} of the WT enzyme with AKG was $3 \pm \{6\}$ s^{-1} (Table 1). The K_M for the WT enzyme with AKG was $\{1{,}098\} \pm 3$ µM, and the k_{sp} was $0.003 \pm \{0.008\} \times 10^6$ $M^{-1}s^{-1}$. By contrast, the k_{cat} of the mutant enzyme with AKG was 0.19 ± 0.01 s^{-1} (Table 2). The K_M for the mutant enzyme with AKG was $\{666.2\} \pm 0.1$ µM, and the k_{sp} was $0.00028 \pm 0.00003 \times 10^6$ $M^{-1}s^{-1}$. Catalytic activity of both enzymes is substantially lowered with the alternative substrate. However, the unreasonably high errors in k_{cat} and k_{sp} for the WT enzyme suggest that the data is not a good fit (Table 1). The measurements for k_{cat}, k_{sp}, and K_M for the WT are unreliable. Likewise, the plot of K_{obs} versus concentration of AKG did not yield the expected curve (Fig. 11*C*). The magnitude of the decrease in k_{cat} with AKG for the WT enzyme was significantly less than expected, supporting the conclusion that the data is essentially erroneous (14). The mutant with AKG data, on the other hand, has relatively well determined constants, suggesting that the mutant is more effective on AKG than is the WT (Table 2). The non-linear curve fit was also appropriate for the mutant with AKG (Fig. 11*D*). As predicted, the smaller side chain of serine likely expanded the region for substrate binding in the active site cleft of hMDH1. Experimentation with other substrates, including pyruvate, hydroxypyruvate, and phenylpyruvate, should be performed to further assess the substrate recognition properties of the mutant (14).

The Pro110Ser mutant of hMDH1 achieves a higher turnover number with the endogenous substrate, OAA. This occurs at the cost of substrate specificity, however, as the specificity constant for the WT is roughly two times that of the mutant. Replacement of proline with serine likely destabilizes the enzyme-substrate complex, leading to a faster dissociation of OAA to malate. To conclude, the WT enzyme differentiates between OAA and AKG more effectively than does the mutant. However, Pro110Ser hMDH1 is more active than the WT with OAA. In addition, the mutant enzyme is likely a better catalyst with the alternative substrate, AKG, as indicated by the reasonable kinetic constants (Table 2). Substrate binding to the enzyme active site is essential for

catalysis. Mutation of Pro-110 decreases specificity for OAA and confers greater turnover with an alternative substrate, AKG. These studies suggest that Pro-110 plays a role in the strict substrate specificity of hMDH1. Experiments aimed to reduce hMDH1 activity and likewise halt glycolysis in proliferating cancer cells might look to manipulate Pro-110.

Experimental procedures

Bacterial culture

Escherichia coli BL21(DE3) cells containing the protein production plasmid (pET28a) that encodes the cytoplasmic human malate dehydrogenase, hMDH1, were provided by Jessica Bell (Department of Chemistry and Biochemistry at the University of San Diego). pET28a encodes isoform 3 of hMDH1. To harvest large quantities of *E. coli* bacteria, liquid cultures were started from a single colony on a streaked plate. *E. coli* BL21(DE3) strains were grown in Luria base (LB) medium at 28°C with shaking (250 rpm). The LB medium was comprised of 1% tryptone, 0.5% yeast extract and 1% NaCl. The medium was supplemented with kanamycin at 50 μg/mL.

WT plasmid isolation

A plasmid miniprep was performed to extract hMDH1 isoform 3 pET28a plasmid DNA from *E. coli* BL21(DE3) cells. The procedure was adapted from Zyppy Plasmid Miniprep Kit instructions from Zymo Research (Irvine, CA). hMDH1 pET28a cells (6 mL) were processed according to the manufacturer's instructions. The column was eluted with 10 mM Tris-HCl, pH 8.5 and 0.1 mM EDTA. To increase DNA yield, the elution buffer was pre-warmed to 50°C, and the incubation period was increased to 20 minutes. A NanoDrop spectrophotometer was used to assess the purity of the plasmid DNA at absorbances of 260 nm and 280 nm. The DNA concentration was also measured.

Plasmid DNA restriction analysis

After extracting hMDH1 isoform 3 pET28a DNA, the DNA was analysed via restriction enzyme mapping. A double digest was performed. A virtual restriction enzyme digest was first run with the enzymes XhoI and ClaI to determine the expected fragment sizes. Benchling, a bioinformatics platform, was used for this purpose. The 50 μL restriction digest comprised CutSmart NEB buffer (50 mM potassium acetate, 20 mM Tris-acetate, 10 mM magnesium acetate, 100 μg/ml BSA, pH 7.9 at 25°C), 10 units each of restriction enzymes XhoI and ClaI, and about 630 ng of DNA. The mixture was incubated at 37°C for about 30 minutes. Once 10 μL of NEB gel loading blue dye (2.5% Ficoll®-400, 11 mM EDTA, 3.3 mM Tris-HCl, pH 8.0 at 25°C, 0.017% SDS, and 0.015% bromophenol blue) were added to 50 μL of restriction digest, the resulting mixture was loaded onto a 1% agarose gel prepared with SybrSafe in Tris-borate-EDTA (89 mM Tris, 89 mM boric acid, and 2 mM EDTA, pH 8.0). An NEB Quick-Load Purple 1 kb plus DNA Ladder was loaded onto the gel. The gel was placed on the transilluminator for detection. The DNA bands were analysed and compared to the virtual digest to confirm the existence of the pET28a plasmid.

Site-directed mutagenesis: PCR

Site-directed mutagenesis was employed for amino acid substitution. Specifically, a proline amino acid residue located at position 110 in hMDH1 isoform 3 was replaced with serine. Mutagenic primers were used to PCR amplify the plasmid expressing the hMDH1 gene (pET28a), inducing a substitution mutation in the process. The primers were designed using Benchling and NEBase changer. The forward primer sequence was GGGCTCCATGAGCAGAAGGGAAG, and the reverse primer sequence was ACAAGAATGGCCACATCC. The Q5 site-directed mutagenesis kit prepared by New England BioLabs (NEB) was used in the PCR. PCR was performed in a total volume of 25 μL containing 0.5 μM of each primer, 25 ng of DNA, and Q5 hot start high-fidelity Master Mix. The thermocycler was programmed to 98°C for 30 seconds to initiate denaturation. Next, 25 PCR cycles were completed at 98°C for 10 seconds, 61°C for 30 seconds, and 72°C for 20 seconds. The final extension period lasted 2 minutes at 72°C. DNA agarose gel

electrophoresis was conducted using a 0.8% agarose gel with SybrSafe in Tris-borate-EDTA (TBE). PCR samples were prepared for electrophoresis by mixing 2 µL of NEB gel loading blue dye with 10 µL of PCR reaction mixture. An NEB Quick-Load Purple 1 kb DNA Ladder was loaded onto the gel. The gel was placed on the transilluminator for detection. The band of the DNA was observed to determine the size of the amplified fragment and to verify the amplification of the template.

Site-directed mutagenesis: transformation

A kinase, ligase, and Dpnl (KLD) treatment was completed to introduce the mutant plasmid into competent NEB 5α *E. coli* cells. The kinase phosphorylated the 5' end of the plasmid expressing the mutant hMDH1 gene (pET28a), and the ligase sealed the nick to produce the circularized plasmid. The restriction enzyme DpnI digested the original template plasmid that did not contain the mutation. The reaction was performed in a total volume of 10 µL containing KLD reaction buffer, KLD enzyme mix, and 25 ng of hMHD1 mutant plasmid PCR product. The resulting solution was incubated at room temperature for about 5 minutes. The KLD mixture (5 µL) was added to 50 µL of thawed NEB 5α competent *E. coli* cells. The resulting mixture was placed on ice for about 40 minutes. The cells were heat shocked at 42°C for 30 seconds and placed on ice for 5 minutes. Room temperature SOC media (950 µL) was added to the mixture, which was incubated at 37°C for about 1 hour with shaking (250 rpm). Onto one LB + kanamycin plate, 100 µL of cells were spread. The remaining cells were centrifuged at 3,000 × g for 3 minutes. Virtually all of the supernatant was removed, and the pellet was resuspended. Resuspended cells (100 µL) were spread onto another LB + kanaycin plate. Both plates were incubated overnight at 37°C.

Mutant plasmid miniprep

A plasmid miniprep was performed to extract the potential mutant plasmid hMDH1 isoform 3 pET28a plasmid DNA from NEB 5α *E. coli* cells. The procedure was adapted from Zyppy Plasmid Miniprep Kit instructions from Zymo Research (Irvine, CA). Mutant hMDH1 pET28a cells (3 mL) were processed according to the manufacturer's instructions, as described previously. The DNA was resuspended in 30 µL of water. The resulting substitution mutation was verified by DNA sequencing with GeneWiz.

Bacterial transformation

The plasmid encoding the gene for the genetically modified human cytosolic malate dehydrogenase isoform 3 was introduced to XJb (DE3) bacterial cells, prepared by Zymo Research (Irvine, CA). Mutant hMDH1 plasmid DNA (144 ng) was added to 50 µL of Z-competent XJb (DE3) cells. Following a 10-minute incubation period, four volumes of room temperature SOC media (208 µL) was added. The resulting mixture was incubated for 1 hour at 37°C with gentle shaking (150 rpm). The cells were spun down at 3,000 × g for 3 minutes. The supernatant was removed (150 µL), and the pellet was resuspended. Resuspended cells (100 µL) were spread onto an LB and kanamycin plate. After about 15 minutes, the plate was inverted and incubated overnight at 37°C.

WT hMDH1 isoform 3 protein overexpression

The bacterial transformation of XJb (DE3) bacterial cells was followed by overexpression, in which the wildtype (WT) hMDH1 isoform 3 plasmid gene was used by the host bacterium to transcribe mRNA, followed by translation into protein. Liquid cultures were started from a single hMDH1 isoform 3 colony on a streaked plate. *E. coli* XJb (DE3) strains, prepared by Zymo Research (Irvine, CA), were grown in Luria base (LB) medium at 37°C with shaking (250 rpm). The media was supplemented with kanamycin at 50 µg/mL. The OD_{600} was between 4.0 and 5.0 at the final stationary growth phase. The starter culture was expanded by adding 1 mL to 50-mL of LB and kanamycin in a 250-mL baffled flask. The culture was then incubated for 2 hours at 37°C until the density reached an OD_{600} of about 0.55-0.6. Once the appropriate OD was reached, cells were cooled to room temperature, followed by induction with IPTG to a final concentration of 0.5 mM. Arabinose was also added to a final concentration of 3 mM. Cells were grown

overnight with vigorous shaking (250 rpm) at 20°C. Cells were harvested the following day by centrifugation at 3,000 × g for 10 minutes at 10 ˚C. Since a freeze-thaw cycle is critical to cell lysis, cells were frozen at −20 °C in advance of lysis.

Cell lysis with WT and mutant protein

Cells overexpressing the WT hMDH1 isoform 3 protein were lysed to obtain a lysate that could be used to purify the protein by nickel affinity (Ni-NTA) chromatography. Cells were removed from the −20°C freezer and thawed on ice. Cells were resuspended in approximately 3 mL/g cell pellet of lysis buffer (20 mM Tris, 100 mM NaCl, pH 8.0) to which a cocktail of protease inhibitors was added. One tablet of Pierce protease inhibitor mini-tablets was dissolved per 10 mL of lysis buffer. The pellet was resuspended. To expedite the cell lysis process, lysozyme was added to a final concentration of 50 µg/mL. DNAse I (60 units) was also added. The resulting mixture was incubated for 30 minutes at 37°C with shaking (200 rpm). The sample was centrifuged at 21,130 × g for 5 minutes at 4°C. The supernatant was removed and centrifuged at 21,130 × g for 15 minutes at 4°C. Cells overexpressing the mutant hMDH1 isoform 3 protein were lysed in the same manner in order to obtain a lysate that could be used to purify the protein by Ni-NTA chromatography.

WT and mutant protein purification

Nickel affinity chromatography was employed to purify the WT hMDH1 isoform 3 protein. Clarified cell lysate from an expression culture was used in this experiment. A variation of the batch method listed in ThermoScientific's protocol for the HisPur Ni-NTA resin (Catalog #88221) was used. The total volume of settled resin was 2 mL. The resin was equilibrated in two resin-bed volumes of equilibration buffer (PBS, 20 mM sodium phosphate, 300 mM sodium chloride, pH 8). The entire cell lysate containing the WT hMDH1 isoform 3 protein was added to the resin and mixed on an end-over-end rotator for 15 minutes at 4°C. The flow-through was then collected. The column was washed with wash buffer (PBS with 25 mM imidazole) until the absorbance at 280 nm reached 0.1. The bound WT hMDH1 protein was eluted with two resin-bed volumes (4 mL) of PBS containing 250 mM imidazole. The absorbance was again measured at 280 nm. The mutant hMDH1 isoform 3 protein was purified the same way, only cell lysate containing the mutant was used.

BCA assay

A bicinchoninic (BCA) assay was performed to determine the protein concentrations of the WT and mutant hMDH1 (15). A BCA assay kit from Pierce Chemical Company (Pierce, Product #23209) was used. The instructions were followed exactly, only the sample and working reagent volumes were halved. In addition, the working reagent was prepared in a 50:2 ratio of reagent A to reagent B.

SDS-PAGE

SDS-PAGE was performed to determine the molecular weight of both the WT and the mutant hMDH1 proteins and to assess the success of the BCA purification procedure. The methods of Laemmli were followed with minor changes (16). A 12% separating gel was prepared. A 4% stacking gel was prepared. The sample buffer was comprised of 31.25 mM Tris (pH 6.8), 1% SDS, 12.5% glycerol, 0.005% bromophenol blue, 2.5% β-mercaptoethanol. The protein samples were immersed in boiling water for 30 minutes. Electrophoresis was carried out at 200 V for 45 minutes. The completed gel was stained overnight in Coomassie Blue stain staining solution containing 0.025% Coomassie Blue R-250, 40% methanol, and 7% acetic acid. The stained gel was then destained in a solution consisting of 40% methanol, 7% acetic acid, and 3% glycerol.

Enzyme kinetics

Several kinetics experiments were performed to assess the activities of both the WT and the mutant hMDH1 proteins in the presence of the native substrate, oxaloacetate (OAA), and an alternative substrate, α-ketoglutarate (AKG). The reaction catalyzed by MDH, namely the conversion of malate to oxaloacetate, was run in

reverse. Consumption of NADH over time was monitored spectrophotometrically. A routine WT hMDH1 assay with OAA and NADH was first performed. The Cary-50 UV-Vis Spectrophotometer was zeroed at 340 nm. The assay was conducted with variable OAA concentrations (5–315 µM), a constant NADH concentration of 0.166 mM, and 99.2 mM potassium phosphate buffer (pH 8). The WT hMDH1 enzyme concentration was 1.03 nM. The oxidation of NADH was observed by measuring the decrease in absorbance at 340 nm. The assay was linear for one minute. The NADH solution was kept at room temperature throughout the assay and the substrate solutions were kept on ice. The assay was performed identically for the WT enzyme with the alternative substrate, α-ketoglutarate (AKG), only the 3,000 µL reaction mixture comprised 513 nM of enzyme, 0.149 mM NADH, 90.0 mM potassium phosphate buffer (pH 8), and a range of AKG concentrations from 4.8 to 3,000 µM. The kinetics of the mutant enzyme were also studied. For the experiment with OAA, the 3,000 µL reaction mixture was comprised of 3.5 nM of the mutant hMDH1 protein, 0.166 mM NADH, 98.7 mM potassium phosphate buffer (pH 8), and an OAA concentration range from 4.8 to 300 µM. Finally, for the mutant enzyme with AKG, the 3,000 µL reaction mixture was comprised of 369 nM mutant hMDH1, 0.149 mM NADH, 90.0 mM potassium phosphate buffer (pH 8), and OAA ranging in concentration from 480 to 3,000 µM.

Acknowledgements— We would like to thank Dr. Jessica Bell, University of San Diego, for providing the E. coli BL21(DE3) cells containing the pET28a plasmid expressing hMDH1. We thank New England BioLabs for providing supplies to run the restriction analysis. Similarly, we thank the Pierce Chemical Company for providing the BCA assay kit as well as the mini-tablet inhibitors. We also thank the MCC (MDH CURE Community) for inviting Providence College to join the program. We thank Dr. Joseph Provost, University of San Diego, for constructing the MDH models used for in silico mutagenesis. We also thank the Department of Biology at Providence College, and Dr. Brett Pellock in particular for his continual support and for allowing us to use his lab equipment. Likewise, we thank the Department of Chemistry and Biochemistry and the chair of the department, Dr. Kenneth T. Overly, for his encouragement and support throughout this process. We thank Providence College undergraduates Colby Agostino, Ethan Dionne, and Frankie Radics for their kinetics data for the WT hMDH1 with OAA. We also thank all members of the CHM 310L course.

References

1. Vander Heiden, M.G., Cantley, L.C., and Thompson, C.B. (2010) Understanding the Warburg Effect: The Metabolic Requirements of Cell Proliferation. *Science*. **324,** 1029–1033.

2. Crabtree, H.G. (1929) Observations on the carbohydrate metabolism of tumours. *Biochem J.* **23,** 536–545.

3. Mansouri, S., Shahriari, A., Kalantar, H., Moini Zanjani, T., and Haghi Karamallah, M. (2017) Role of malate dehydrogenase in facilitating lactate dehydrogenase to support the glycolysis pathway in tumors. *Biomed Rep.* **6,** 463–467.

4. Hanse, E.A., Ruan, C., Kachman, M., Wang, D., Lowman, X.H., and Kelekar, A. (2017) Cytosolic malate dehydrogenase activity helps support glycolysis in actively proliferating cells and cancer. *Oncogene*. **36,** 3915–3924.

5. Yu, L., Chen, X., Sun, X., Wang, L., and Chen, S. (2017) The Glycolytic Switch in Tumors: How Many Players Are Involved? *J Cancer.* **8,** 3430–3440.

6. Borst, P. (2020) The malate-aspartate shuttle (Borst cycle): How it started and developed into a major metabolic pathway. *IUBMB Life*. **72,** 2241–2259.

7. The PyMOL Molecular Graphics System, Version 2.0 Schrödinger, LLC.

8. Wolfram Research, Inc. (www.wolfram.com), Mathematica Online, Champaign, IL (2020).

9. Bell, J.K., Yennawar, H.P., Wright, S.K., Thompson, J.R., Viola, R.E., and Banaszak, L.J. (2001) Structural analyses of a malate dehydrogenase with a variable active site. *J. Biol. Chem.* **276**, 31156–31162.

10. Benchling [Biology Software]. (2021).

11. Rath, A., Glibowicka, M., Nadeau, V.G., Chen, G., and Deber, C.M. (2009) Detergent binding explains anomalous SDS-PAGE migration of membrane proteins. *Proc. Natl. Acad. Sci. U.S.A.* **106**, 1760–1765.

12. Ding, Y., and Ma, Q.H. (2004) Characterization of a cytosolic malate dehydrogenase cDNA which encodes an isozyme toward oxaloacetate reduction in wheat. *Biochimie*. **86,** 509–518.

13. Johnson, K.A. (2019) New standards for collecting and fitting steady state kinetic data. *Beilstein J. Org. Chem*. **15,** 16–29.

14. Wright, S.K., and Viola, R.E. (2001) Alteration of the Specificity of Malate Dehydrogenase by Chemical Modulation of an Active Site Arginine. *J. Biol. Chem*. **33,** 31151–31155.

15. Smith, P.K., Krohn, R.I., Hermanson, G.T., Mallia, A.K., Gartner, F.H., Provenzano, M., Fujimoto, E.K., Goeke, N.M., Olson, B.J. and Klenk, D.C. (1985) Measurement of protein using bicinchoninic acid. *Anal. Biochem*. **150,** 76–85.

16. Laemmli, U.K. (1970) Cleavage of Structural Proteins during the Assembly of the Head of Bacteriophage TM4. *Nature*. **227**, 680–685.